Effect of passive structure and toroidal rotation on resistive wall mode stability in the EAST tokamak*

Liu Guang-Jun(刘广君)[a)b)], Wan Bao-Nian(万宝年)[a)], Sun You-Wen(孙有文)[a)], Liu Yue-Qiang(刘钺强)[c)], Guo Wen-Feng(郭文峰)[a)], Hao Guang-Zhou(郝广周)[d)], Ding Si-Ye(丁斯晔)[a)], Shen Biao(沈 飙)[a)], Xiao Bing-Jia(肖炳甲)[a)], and Qian Jin-Ping(钱金平)[a)†]

[a)] *Institute of Plasma Physics, Chinese Academy of Sciences, Hefei* 230031, *China*
[b)] *b) Luoyang Optoelectro Technology Development Center, Luoyang* 471009, *China*
[c)] *Euratom/UKAEA Fusion Association, Culham Science Centre, Abingdon, OX14 3DB, United Kingdom*
[d)] *Southwestern Institute of Physics, Chengdu* 610041, *China*

(Received 7 November 2013; revised manuscript received 26 December 2013; published online 22 May 2014)

If β_N exceeds $\beta_N^{no-wall}$, the plasma will be unstable because of external kink and resistive wall mode (RWM). In this article, the effect of the passive structure and the toroidal rotation on the RWM stability in the experimental advanced superconducting tokamak (EAST) are simulated with CHEASE and MARS codes. A model using a one-dimensional (1D) surface to present the effect of the passive plate is proved to be credible. The no wall β_N limit is about $3l_i$, and the ideal wall β_N limit is about $4.5l_i$ on EAST. It is found that the rotation near the $q = 2$ surface and the plasma edge affects the RWM more.

Keywords: resistive wall mode, passive structure, rotation

PACS: 52.55.Fa, 52.35.Qz, 52.65.Kj **DOI:** 10.1088/1674-1056/23/7/075205

1. Introduction

For economical and environmental friendly thermonuclear energy production, a tokamak requires[1,2] the following to achieve the ignition condition; the energy confinement time τ_E should be large enough; a sufficient volume average toroidal beta β_T is necessary for adequate fusion power density; and a significant self-driven bootstrap current fraction f_{BS} is requisite for the steady-state operation. Here $\beta_T = 2\mu_0\langle p\rangle/B_T^2$, where $\langle p\rangle$ is the average pressure in the plasma area, and B_T is the toroidal magnetic field. And $f_{BS} = I_{BS}/I_p \propto \varepsilon^{1/2}\beta_p$, where ε is the inverse aspect ratio a/R, a and R are the minor radius and the major radius, respectively, $\beta_p = 2\mu_0\langle p\rangle/B_p^2$, and B_p is the poloidal magnetic field . Because of $\beta_T^*\beta_p = \beta_N^2(1+\kappa^2)/8$, both the requirements of high β_T and high f_{BS} lead to the requirement of high β_N. One of the main goals of the advanced tokamak research is to obtain β_N significantly larger than three. There are some operational scenarios that have been identified to have the potential for a steady-state high confinement, high beta operation:[1] (i) the radiative I mode, (ii) the high l_i regime, and (iii) the negative or weak central magnetic shear regime.

The resistive wall mode (RWM) has long been thought of as an instability that ultimately limits the pressure of the plasma.[3] In tokamak devices, when β_N is larger than the no wall beta limit $\beta_N^{no-wall}$, the pressure gradient will drive an ideal MHD instability, the external kink mode (XK), whose growth time is on the order of microsecond scale. The XK mode will be stabilized by an ideal wall (which is not far from the plasma), but a finite resistive wall will transform the mode to the RWM and reduce the mode growth time to the wall time scale; that is, on the order of milliseconds.

One of the most important missions of the experimental advanced superconducting tokamak (EAST) is to demonstrate high performance and steady state operation in ITER-like plasma configuration with superconducting equilibrium field coils.[4,5] In the last experimental campaign on EAST, the normalized poloidal β (about 1) was much lower than the predicted no wall limit. In the next experimental campaign, the heating power of EAST will be 1 MW ECRH, 12 MW ICRF, 4 MW NBI,[6] and 10 MW LHCD. As the heating power increases, the poloidal beta is likely to exceed the no wall beta limit and trigger the RWM. It is necessary to make some predictions about the RWM on EAST: the effect of the passive plate on the RWM, the no wall and ideal wall beta limits, and the effect of plasma rotation on the RWM.

In this article, the study of the external kink and the RWM on EAST will be modeled by using the cubic hermite element axisymmetric static equilibrium (CHEASE) code[7] and the MARS code.[8–10] In next section, the passive structure of EAST and the one-dimensional (1D) model for the passive plate will be presented, with the results of the simulation.

*Project supported by the National Magnetic Confinement Fusion Science Program of China (Grant Nos. 2012GB105000, 2011GB101000, 2011GB107000, and 2013013GB102000) and the National Natural Science Foundation of China (Grant Nos. 10725523, 10721505, 10090212, 111005037, and 11205199).

†Corresponding author. E-mail: jpqian@ipp.ac.cn

© 2014 Chinese Physical Society and IOP Publishing Ltd

2. Passive structure of EAST and 1D model of the passive plate

2.1. Passive structure on EAST

The EAST passive structure is designed to be up–down symmetric, as shown in Fig. 1. Figure 1 shows the the structures of the passive plate, the divertor targets, and the limiter.[4,5,11] The passive plates are made of copper segments. Each loop has eight segments of 30 mm in thick and 350 mm in width, which are connected to adjacent ones by the supporting structures and the vacuum vessel. The double-layer vacuum vessel is made of 8 mm thick stain-less steel plates.[12,13]

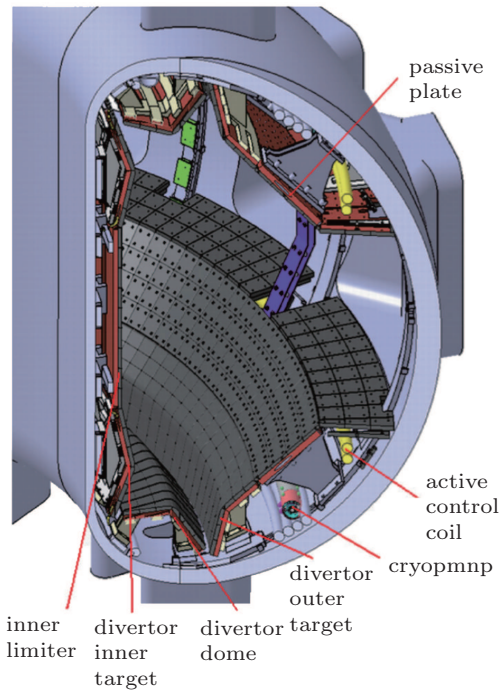


Fig. 1. (color online) Cross section of the passive structure on EAST tokamak.

The wall time constant is defined as

$$\tau_{\rm w} = \mu_0 \sigma r \delta_{\rm w}, \tag{1}$$

where σ, r, and $\delta_{\rm w}$ are the conductivity, the position of the passive structure, and the thickness of the passive structure, respectively. The wall time constants of three parts of the passive structure on EAST are listed in Table 1.

Table 1. The wall time constants on EAST.

Wall	Inner vessel	Outer vessel	Passive plate
$\tau_{\rm w}$/ms	14.335	15.23	1.25

2.2. The 1D model of the passive plate

As shown above, the passive plate has a complex structure: it is asymmetric in the toroidal direction and unconnected in the poloidal direction. For ease of calculation, a 1D model will be used to simulate the passive plate later. A benchmark is necessary to evaluate whether this 1D model using the positive shear equilibrium is credible in later sections.

In the simulation, a conformal wall whose shape is similar to that of the plasma boundary will be used as the reference wall. To study the effect of the wall in a high magnetic field, the contrastive wall shown in Fig. 2(a) is designed. In order to simulate the actual situation, the left part of the contrastive wall contacts with the vacuum vessel in the high field. The ideal wall $\beta_{\rm N}$ limit of these two walls and the no wall $\beta_{\rm N}$ limit are compared to each other in positive magnetic shear equilibrium, and the result is presented in Fig. 2(b). Since there is little different between the two wall's ideal $\beta_{\rm N}$ limits, this infers that the wall in the high field has little affect on the ideal wall $\beta_{\rm N}$ limit.

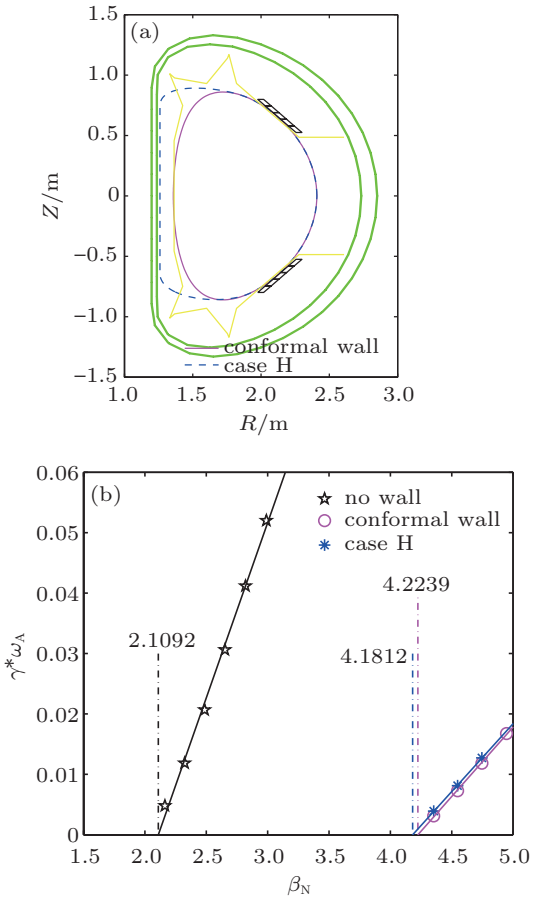


Fig. 2. (color online) Comparison of conformal wall (pink solid line) and contrastive changed high field wall (case H, blue dashed line): (a) shapes of the walls, (b) ideal wall $\beta_{\rm N}$ limits of the walls in positive shear equilibrium.

To study the effect of the wall in a low magnetic field, three contrastive walls shown in Fig. 3(a) are designed. In order to simulate the actual situation, in the area of the passive plate, these walls follow the shape of the passive plate. In the gap between up and down passive plates, the parts of the

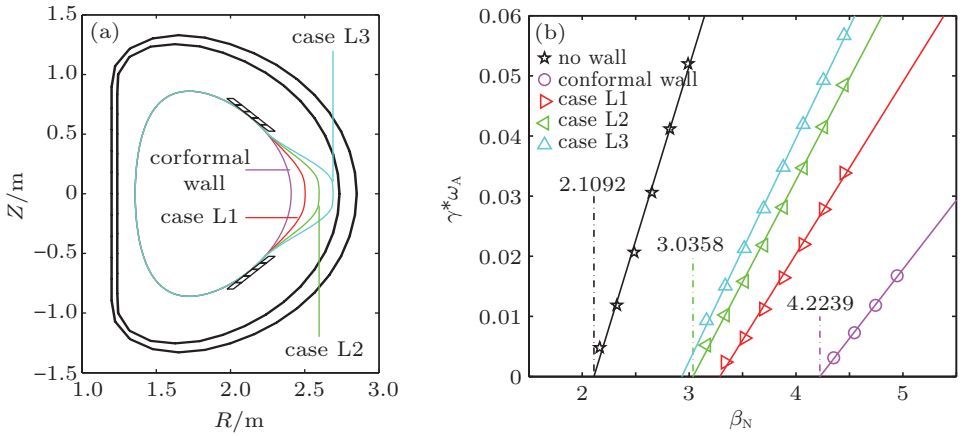


Fig. 3. (color online) Comparison of conformal wall (pink solid line) and contrastive changed low field walls (case L1, case L2, case L3): (a) shapes of the walls, and (b) ideal wall β_N limits of the walls.

contrastive walls are farther and farther away from the plasma, and the wall in case L3 contacts with the vacuum vessel in the low field. Similar to discussing the high field wall, the ideal wall β_N limits are compared. Figure 3(b) makes it clear that the low field wall has a strong affect on ideal wall β_N. However, when the wall changes from case L2 to case L3, the ideal wall β_N limit decreases little.

These results show that in case L2, the passive plate is the dominant part to affect the β_N limit in the whole wall. The resistive wall in case L2 is a good approximation for the passive plate structure.

3. Simulation results

3.1. Different magnetic shear equilibriums

Three equilibriums with positive magnetic shear, weak magnetic shear, and negative central magnetic shear will be simulated by CHEASE based on shot 38300, 4000 ms EAST. The focus of this study is the 2/1 kink mode, so the q profile is designed as follows: $q_a < 5$, $1.6 < q_{min} < 2$. The 2/1 NTM is not taken into consideration. The characteristic parameters of the three different equilibriums ($R_0 = 1.88$ m, $a = 0.413$ m, $B_T = 1.832$ T, $\kappa = 1.637$) are shown in Table 2 and Fig. 4. Figure 4 shows the pressure profiles, the current profiles, and the q profiles of the equilibriums.

Table 2. Characteristic parameters of different magnetic shear equilibriums.

Equilibrium	I_p/kA	β_N	l_i	q_0	q_{min}	$s_{q\,min}$	q_{edge}
Positive shear	425	0.6738	0.7167	1.6999	1.6999	0	4.4877
Weak shear	438	0.7229	0.8224	1.8241	1.8241	0	4.4899
Negative shear	434	0.6502	0.8269	1.9754	1.6656	0.4429	4.4998

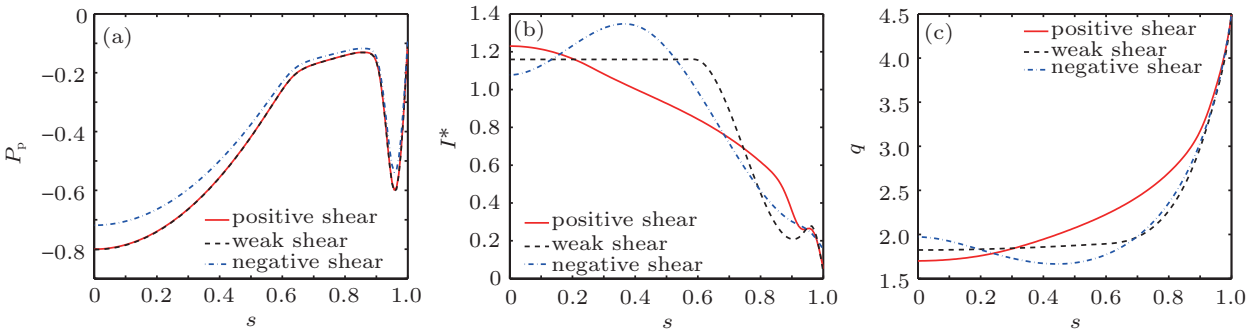


Fig. 4. (color online) Characteristic parameters of positive magnetic shear equilibrium (red solid lines), weak magnetic shear equilibrium (black dashed lines), and negative magnetic shear equilibrium (blue dash-dotted lines): (a) pressure profiles, (b) current profiles, (c) q profiles.

3.2. The β_N limit of different equilibriums

To obtain the β_N limit, it is necessary to fix the I^* profile and magnitude, meanwhile keeping the pressure profile and scanning the pressure magnitude in the CHEASE code. The $\beta_N^{no-wall}$ and $\beta_N^{ideal-wall}$ of the equilibriums in Subsection 3.1 can be obtained by MARS. The results are shown in Table 3. In this table, $\beta_{N,pp}^{ideal-wall}$ and $\beta_{N,vv}^{ideal-wall}$ show the $\beta_{N,max}$ with only ideal passive plate and with only ideal inner vacuum vessel, respectively. Because the vacuum vessel is far away from the plasma on EAST, $\beta_{N,vv}^{ideal-wall}$ is close to $\beta_N^{no-wall}$.

Table 3. The $\beta_{N,max}$ in different equilibriums.

Equilibrium	$\beta_N^{no-wall}$	$\beta_{N,vv}^{ideal-wall}$	$\beta_{N,pp}^{ideal-wall}$
Positive shear	2.1092	2.3179	3.0358
Weak shear	2.6036	2.8816	3.7267
Negative shear	2.6079	2.8275	3.818

According to Strait's paper, $\beta_{N,max}$ is proportional to internal inductivity l_i. Table 4 shows the relationship between $\beta_{N,max}$ and l_i in our study. The no wall β_N limit is about $3l_i$, and the ideal wall β_N limit is about $4.5l_i$.

Table 4. The $\beta_{N,max}/l_i$ in different equilibriums.

Equilibrium	$\beta_N^{no-wall}/l_i$	$\beta_{N,vv}^{ideal-wall}/l_i$	$\beta_{N,pp}^{ideal-wall}/l_i$
Positive shear	2.943	3.2341	4.2358
Weak shear	3.1658	3.5039	4.531528
Negative shear	3.1538	3.4194	4.61742

3.3. Effect of the wall–plasma distance

Figure 5 shows the effect of the wall–plasma distance on the growth rates of resistive modes and ideal kinks in different equilibriums. According to this figure, the stability limit of the ideal wall radius d_{ideal} is about $1.42a$–$1.45a$, where a is the minor radius of the equilibrium. The radius of the inner vacuum vessel, d_{vv}, is always larger than d_{ideal}. With $n \neq 0$, the plasma is stable when $d_{res} < d < d_{ideal}$ for both RWM and ideal kink. Here d_{res} is the stability limit of the resistive wall radius, which is a function of the plasma toroidal rotation. This infers that only with a vacuum vessel, the RWM will be always stable, and the ideal kink will be unstable without another control method on EAST. The behavior of the RWM will mainly depend on the passive plate in the whole passive structure.

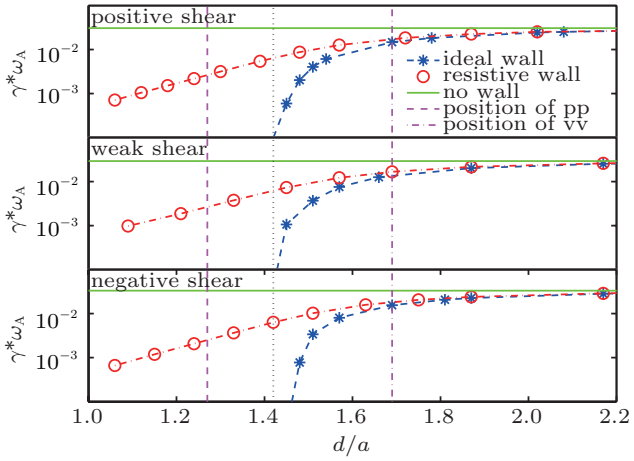


Fig. 5. (color online) Mode growth rates versus the wall–plasma distance.

3.4. Effect of plasma toroidal rotation on EAST

Except for stated explicitly in the later of this paper, the parameters in the simulation are $C_\beta = 0.35$ and $\tau_w = 1.25$ ms for the conformal resistive wall, where $C_\beta = (\beta_N - \beta_N^{no-wall}) / (\beta_N^{ideal-wall} - \beta_N^{no-wall})$, and the positive magnetic shear equilibrium is used.

During the DIII-D experiments[14] in 2005 and the EAST-DIII-D joint experiments in 2013, it was found when the rotation profile is global, it is easy to obtain $\beta_N \simeq 6l_i$ plasma without RWM control. It is speculated that rotations in different areas affect differently the RWM. In Gregoratto's opinion, the rotation near $q = 2$ is important.[15] In Bondeson's view, the rotation near the resonance surfaces is important, and when the rotation is larger enough, the global rotation will be important due to the mode coupling.[16] In this paper, the damping model is the sound wave damping.[17]

3.4.1. Characters of $C_\beta = 0.35$ in positive magnetic shear equilibrium

When $C_\beta = 0.35$, as shown in Fig. 6(a), the $q = 2$ surface and the $q = 3$ surface are near the $s = 0.6$ surface and the $s = 0.91$ surface, respectively. The perturbation displacements and energies have peaks on $q = 2$, $q = 3$, and $q = 4$ surfaces in Fig. 6(b). The perturbation on the $q = 2$ surface is largest because of the mode coupling of $m = 2$ and $m = 3$, and the perturbation in the $q > 2$ area is also large.

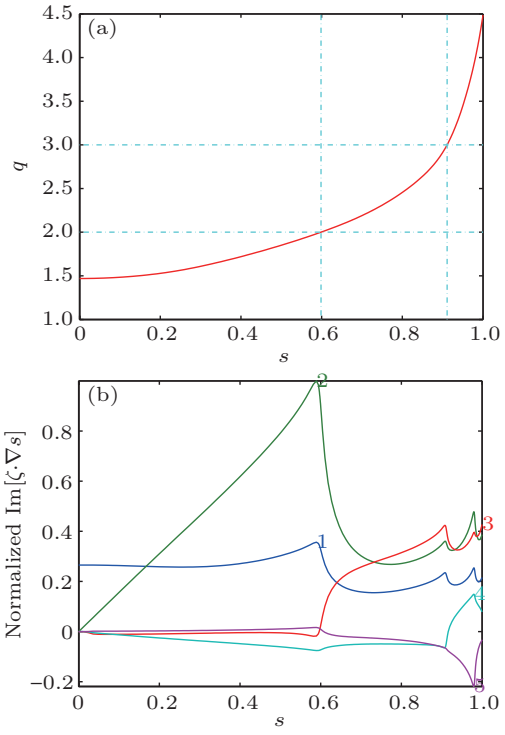


Fig. 6. (color online) The perturbation displacements (a) and energies (b) when $C_\beta = 0.35$ without rotation.

3.4.2. Characters of rotation profiles

Firstly, the rotation profile uniform factor F_Ω is defined as

$$F_\Omega = \frac{1}{\Omega_{max}} \frac{\int \Omega \, dV}{\int dV} \approx \frac{1}{\Omega_{max}} \frac{\int \Omega(s) s \, ds}{\int s \, ds}, \qquad (2)$$

where $s \equiv s(\psi) = \sqrt{(\psi_{\rm edge} - \psi)/(\psi_{\rm edge} - \psi_0)}$, ψ is the poloidal flux, Ω is the plasma toroidal rotation, and $\int x{\rm d}V$ is the volume integration of x.

The product $F_\Omega \Omega_{\rm max}$ of the rotation profile uniform factor F_Ω and the maximum value of rotation profile $\Omega_{\rm max}$ is the total rotation of the plasma.

As shown in Fig. 7, six rotation profiles of Gaussian distribution with $F_\Omega \simeq 0.437$ are designed to study the effects of the rotation on the $q = 2$ surface, the plasma edge area, and the core area. The peaks of these rotations are located at $s_{\Omega,\rm max} = 0$, $s_{\Omega,\rm max} = 0.36$, $s_{\Omega,\rm max} = 0.53$, $s_{\Omega,\rm max} = 0.6$, $s_{\Omega,\rm max} = 0.68$, and $s_{\Omega,\rm max} = 0.8$, respectively. The uniform profile is used for comparison.

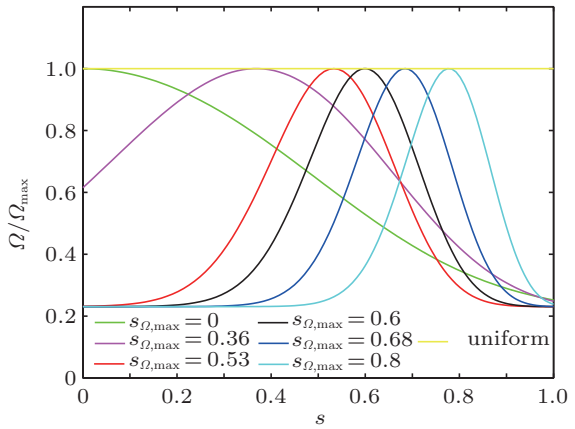


Fig. 7. (color online) Plasma rotation profile in the simulation.

3.4.3. Effect of plasma toroidal rotation

In this section, the effect of the plasma toroidal rotation on the RWM growth rates and frequencies will be discussed by scanning the magnitudes and profiles of rotation. Figure 8 shows the curve of mode growth rates versus plasma rotation in different rotation profiles.

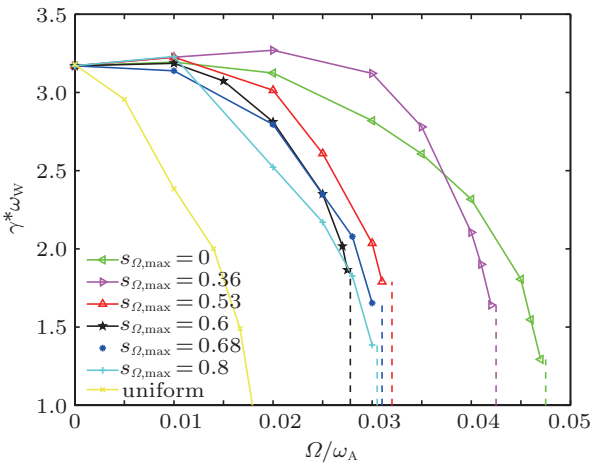


Fig. 8. (color online) Effect of different plasma rotation profiles on the RWM.

Some conclusions can be drawn from Figs. 7 and 8. From a comparison of the three rotation profiles with $s_{\Omega,\rm max} = 0.53$, $s_{\Omega,\rm max} = 0.6$, and $s_{\Omega,\rm max} = 0.68$, it is clear that the critical rotation velocity of the profile with $s_{\Omega,\rm max} = 0.6$ is the lowest. The rotation near the $q = 2$ surface is most important in affecting the RWM. This infers from the comparison of rotation profiles with $s_{\Omega,\rm max} = 0.6$, $s_{\Omega,\rm max} = 0.68$, and $s_{\Omega,\rm max} = 0.8$ that the rotation near the plasma edge is important too. Although the critical rotation velocity of the profile with $s_{\Omega,\rm max} = 0.6$ is the lowest, the critical rotation velocities of the other two profiles are not much higher. The comparison of the rotation profiles with $s_{\Omega,\rm max} = 0$, $s_{\Omega,\rm max} = 0.36$, and $s_{\Omega,\rm max} = 0.6$ shows that the rotation in the plasma core is less important since the critical rotation velocities of the previous two profiles are much higher in Fig. 8.

4. Conclusion

The issues about $n = 1$ RWM are simulated by CHEASE and MARS-F codes based on EAST tokamak. Three points have been discussed.

First, the feasibility and the method to use a 1D model to present the complex passive plate structure has been discussed. It is found that the conducting wall at the high field side affects the RWM instability less, while the conducting wall at the low field side strongly affects the RWM instability.

Second, based on the previous result, $\beta_{\rm N}^{\rm no-wall} \approx 3l_{\rm i}$ and $\beta_{\rm N}^{\rm ideal-wall} \approx 4.5$ are derived with the present passive plate structure on EAST. It is found the $\beta_{\rm N,vv}^{\rm ideal-wall}$ is close to $\beta_{\rm N}^{\rm no-wall}$, while the stability limit of the ideal wall radius $d_{\rm ideal}$ is proven to be always less than the radius of the vacuum vessel, $d_{\rm vv}$. This means that the vacuum vessel will have little affect on the RWM in EAST tokamak.

Third, it is found that the rotation near the $q = 2$ surface is most important to the RWM instability. The rotation in the outer plasma region with $q > 2$ is also important to the RWM instability, mainly due to the coupling between $m = 2$ and $m = 3$ modes. Because of the lack of the $q = 1$ surface, the rotation in the plasma core is less important to the RWM instability.

There are three main issues that remain: (i) because of the complexity of the passive structure on EAST, it is necessary to use a more elaborate model to study the effect of the passive structure; (ii) more kinetic effects should be added to our study of the RWM; and, (iii) the simulation results should be compared with experimental results from EAST in the future.

Acknowledgment

The author is thankful for the help from Prof. Oliver Sauter, Xia Guo-Liang, and Li Li.

References

[1] Taylor T S 1997 *Plasma Physics and Controlled Fusion* **39** B47
[2] Kikuchi M and Azumi M 2012 *Rev. Mod. Phys.* **84** 1807
[3] Chu M S and Okabayashi M 2010 *Plasma Physics and Controlled Fusion* **52** 123001
[4] Wan Y X, Li J G and Weng P D 2006 *21st IAEA Fusion Energy Conf.*, Chengdu, China
[5] Wan B N 2009 *Nuclear Fusion* **49** 104011
[6] Wu B, Wang J F, Li J B, Wang J and Hu C D 2011 *Fusion Engineering and Design* **86** 947
[7] Lütjens H, Bondeson A and Sauter O 1996 *Computer Physics Communications* **97** 219
[8] Liu Y Q, Bondeson A, Fransson C M, Lennartson B and Breitholtz C 2000 *Physics of Plasmas* **7** 3681
[9] Bondeson A, Liu Y Q, Gregoratto D, Gribov Y and Pustovitov V D 2002 *Nuclear Fusion* **42** 768
[10] Xia X N, Liu Y, Liu C, He Y L and Xia G L 2013 *Chin. Phys. B* **22** 055203
[11] Qian J P, Wan B N, Shen B, Walker M L, Humphreys D A and Xiao B J 2009 *Chin. Phys. B* **18** 2432
[12] Ji X, Song Y T, Wu S T, Wang Z B, Shen G, Liu X F, Cao L, Zhou Z B, Peng X B and Wang C H 2012 *Plasma Science and Technology* **14** 855
[13] Liu G J, Wan B N, Qian J P, Sun Y W, Xiao B J, Shen B, Luo Z P, Ji X and Chen S L 2012 *Chin. Phys. B* **21** 085201
[14] Politzer P A, Hyatt A W, Luce T C, Perkins F W, Prater R, Turnbull A D, Brennan D P, Ferron J R, Greenfield C M and Jayakumar J 2005 *Nuclear Fusion* **45** 417
[15] Gregoratto D, Bondeson A, Chu M S and Garofalo A M 2001 *Plasma Physics and Controlled Fusion* **43** 1425
[16] Bondeson A, Liu Y Q, Gregoratto D, Fransson C M and Gribov Y 2003 *Plasma Physics and Controlled Fusion* **45** A253
[17] Chu M S, Greene J M, Jensen T H, Miller R L, Bondeson A, Johnson E W and Mauel M E 1995 *Physics of Plasmas* **2** 2236